Supplementary Information (SI) to accompany

Sorting of molecular shuttles by designing electrical and mechanical properties of microtubules

Naoto Isozaki, Hirofumi Shintaku, Hidetoshi Kotera, Taviare L. Hawkins,

Jennifer L. Ross, and Ryuji Yokokawa*

*Ryuji Yokokawa

Department of Micro Engineering

Kyoto University

Kyoto Daigaku-Katsura, Nishikyo-ku

Kyoto 615-8540, Japan

Tel/Fax: +81-75-383-3682

Email: ryuji@me.kyoto-u.ac.jp

Contents

1. Supporting Information

***L*p measurements.** L_p measurements were based on previous reports using thermal fluctuations of microtubules (MTs).[1-3] Fluctuating MTs were captured as 500 sequential images, and their shapes were detected with FIESTA (Fig. S2a). MTs were divided into >20 segments, and *x*- and *y*-coordinates of those segments were obtained. We did not further analyse the frames when either *x*- or *y*-coordinates at the MT free (right) end deviated over two standard deviations defined by *x*- or *y*-coordinates at the ends of all frames. The path length *s* along an MT was defined as zero at the affixed (left) end of the MT skeleton. The origin of an orthogonal coordinate system was placed at $s = 0$ with the *x*-axis parallel to the tangent line of MT at $s = 0$. MT shape, $y(s)$, in each frame is expressed by $W_n(s/L)$ which is the superposition of sine, cosine, hyperbolic sine, and hyperbolic cosine waves:

$$y(s) = \sum_{n=1}^{\infty} \sqrt{\frac{1}{L}} a_n W_n\left(\frac{s}{L}\right) \tag{S1}$$

and

$$W_n\left(\frac{s}{L}\right) = \frac{-cosh(q_n) - cos(q_n)}{sin(q_n) + sinh(q_n)}\left(sin\left(\frac{q_n s}{L}\right) - sinh\left(\frac{q_n s}{L}\right)\right) + cos\left(\frac{q_n s}{L}\right) - cosh\left(\frac{q_n s}{L}\right). \tag{S2}$$

Here, L is the MT length, and the parameters q_n satisfy

$$cos(q_n)\, cosh(q_n) = -1. \tag{S3}$$

Solutions for equation (S3) are $q_1 \approx 1.875$, $q_2 \approx 4.695$, $q_3 \approx 7.855$, and $q_n \approx (n - 1/2)\pi$ for $n \geq 4$. The decomposed $y(s)$ satisfy the boundary conditions for the clamped and free end of an MT; $y(0) = y'(0) = y''(L) = y'''(L) = 0$. The amplitudes a_n are represented by

$$a_n = \sqrt{\frac{1}{L}} \int_{s=0}^{L} y(s) W_n\left(\frac{s}{L}\right) ds, \tag{S4}$$

which is the Fourier inverse transform of equation (S1). When an MT is divided into $N + 1$ points with the position of (x_k, y_k), the length Δs_k is derived by $\Delta s_k = \{(x_{k+1} - x_k)^2 + (y_{k+1} - y_k)^2\}^{1/2}$. The equation (S4) can be approximately solved by the midpoint method as

$$a_n \approx \sqrt{\frac{1}{L}} \sum_{k=1}^{N} y_k \Delta s_k W_n\left(\frac{s_k^{mid}}{L}\right), \quad n = 1, \ldots, N-1 \tag{S5}$$

where

$$L = \sum_{k=1}^{N} \Delta s_k \tag{S6}$$

and

$$s_k^{mid} = \Delta s_1 + \Delta s_2 + \Delta s_3 + \cdots + \Delta s_{k-1} + \frac{1}{2}\Delta s_k. \quad \text{(S7)}$$

The equation (S5) was solved under N = 12. The MT skeleton was expressed by substituting a_n into equation (S1) as shown in Fig. S2a. The bending energy U of the MT was calculated by

$$U = \frac{1}{2}\kappa \sum_{n=1}^{\infty} \left(\frac{q_n}{L}\right)^4 (a_n - a_n^0)^2 \quad \text{(S8)}$$

where κ is MT flexural rigidity and a_n^0 is the amplitude of the initial shape of the MT in the absence of thermal energy. From the equipartition theorem, each quadratic term in equation (S8) contributes an average thermal energy, $1/2k_BT$. Since κ can be expressed by L_p; $\kappa = L_p k_B T$, L_p was calculated with the variance of amplitude in each mode;

$$L_p = \frac{1}{var(a_n)} \left(\frac{L}{q_n}\right)^4. \quad \text{(S9)}$$

Figure S2b is the plot of $L^4/\mathrm{var}(a_n)$ and q_n^4. In lower modes q_n ($n \leq 6$), they had a linear relationship as indicated by equation (S9). However, plots of higher modes q_n ($n > 6$) were not linearly dependent. This was because the shot and thermal noises of electrons in a CMOS image sensor were more dominant than MT fluctuations in higher modes. We found the range of noise-dominant modes by measuring correlation coefficients, r, between $L^4/\mathrm{var}(a_n)$ and q_n^4; once r dropped below 0.95, the mode or larger modes were regarded as noise-dominant modes. We calculated the mean ± SD of L_p with removing the noise-dominant modes from the calculation.

Correlation time. Mode amplitudes will transfer into the steady-state phase after a correlation time. The correlation time, τ_n, is represented by

$$\tau_n = \frac{\gamma}{L_p k_B T} \left(\frac{L}{q_n}\right)^4 \quad \text{(S10)}$$

where γ is the apparent perpendicular drag coefficient for the MT. The γ value is reported to be calculated by

$$\gamma = \gamma_0 + \varepsilon_0 \left(\frac{q_n}{L}\right)^4 \quad \text{(S11)}$$

where γ_0 is the perpendicular drag coefficient for the MT without internal friction within the MT and ε_0 depends on the amount of internal friction and the radius of the MT.[3] They were experimentally derived as γ_0 = 0.011 s N m^{-1} and ε_0 = 6.9 × 10^{-25} s N m^2. Correlation times (τ_n) should be less than the sampling time (= 0.4 s in our measurement system) to make successive MT shapes independent of each other. The average length of MT-1 to MT-5 ranged over 6.7–7.6 × 10^{-6} m. By substituting the upper limit of τ_n (= 0.4 s), the maximum L (= 7.6 × 10^{-6} m), and the minimum q_n (= 1.875 at n = 1) into equations (S10,11), we obtained the lower limit of measurable L_p as 2.2 mm. Our measured L_p,

3.2–17 mm, satisfied this limitation. In the case of longer or softer MTs, we need to increase the sampling time to correspond with MT length and stiffness.

2. Supplementary Figures

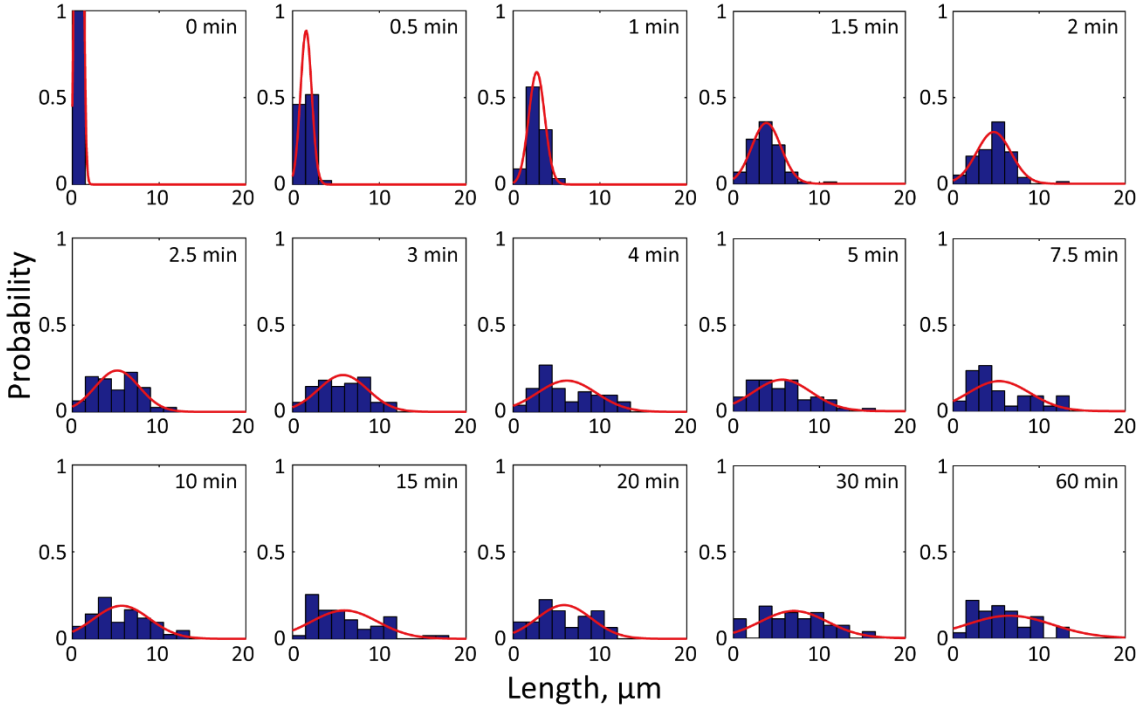

Supplementary Figure 1. | Histogram of MT length at each sampling time. The tubulin concentration is 30 μM in this example. Each probability distribution is normalized so that the area under the curve is one (n = 6 measurements for 0 min, n = 89 for 0.5, 1, and 1.5 min, n = 81 for 2 min, n = 79 for 2.5 min, n = 55 for 3 min, n = 52 for 4 min, n = 61 for 5 min, n = 34 for 7.5 and 60 min, n = 42 for 10 min, n = 55 for 15 min, n = 31 for 20 min, and n = 27 for 30 min incubation time). Each distribution was fit to a Gaussian function, $f(L)$, as a red line:

$$f(L) = \frac{1}{\sigma\sqrt{2\pi}} \exp\left(-\frac{(L-\mu)^2}{2\sigma^2}\right) \tag{S12}$$

to find the mean (μ) and standard deviation (σ) (R^2 = 1.00 for 0 min, R^2 = 0.99 for 0.5, 1, and 1.5 min, R^2 = 0.93 for 2 min, R^2 = 0.77 for 2.5 min, R^2 = 0.83 for 3 min, R^2 = 0.46 for 4 and 15 min, R^2 = 0.76 for 5 min, R^2 = 0.43 for 7.5 min, R^2 = 0.73 for 10 min, R^2 = 0.58 for 20 min, R^2 = 0.59 for 30 min, and R^2 = 0.53 for 60 min). Lilliefors tests found the non-normality of histograms at 2.5, 4, 7.5, 15, and 60 min incubation time at a critical value of $p < 0.05$. Bin width = 1.5 μm.

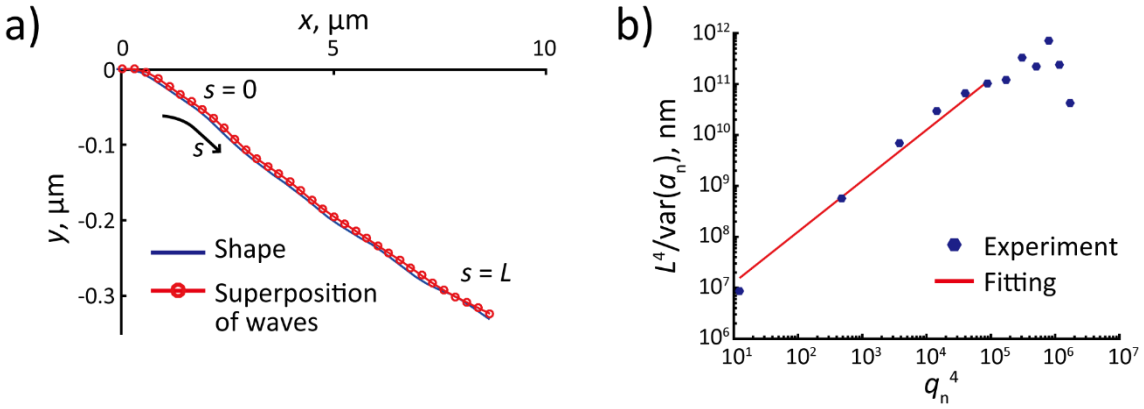

Supplementary Figure 2. | Details for measuring L_p of MTs. (**a**) Example of Fourier decomposition of MT shape for a single frame. The shape $y(s)$ (blue line) is expressed by a superposition of waves (red circles and line), which consist of sine, cosine, hyperbolic sine, and hyperbolic cosine (see Supporting Information for details). L: length of a free segment. (**b**) Relationship between $L^4/\mathrm{var}(a_n)$ and q_n^4. q_n corresponds to the mode numbers. The experimental results are represented by blue dots. The first few modes were fit to equation (S9) as a red line ($R^2 = 0.99$), $L^4/\mathrm{var}(a_n)$ was proportional to q_n^4 with an increase of L_p due to low noise.

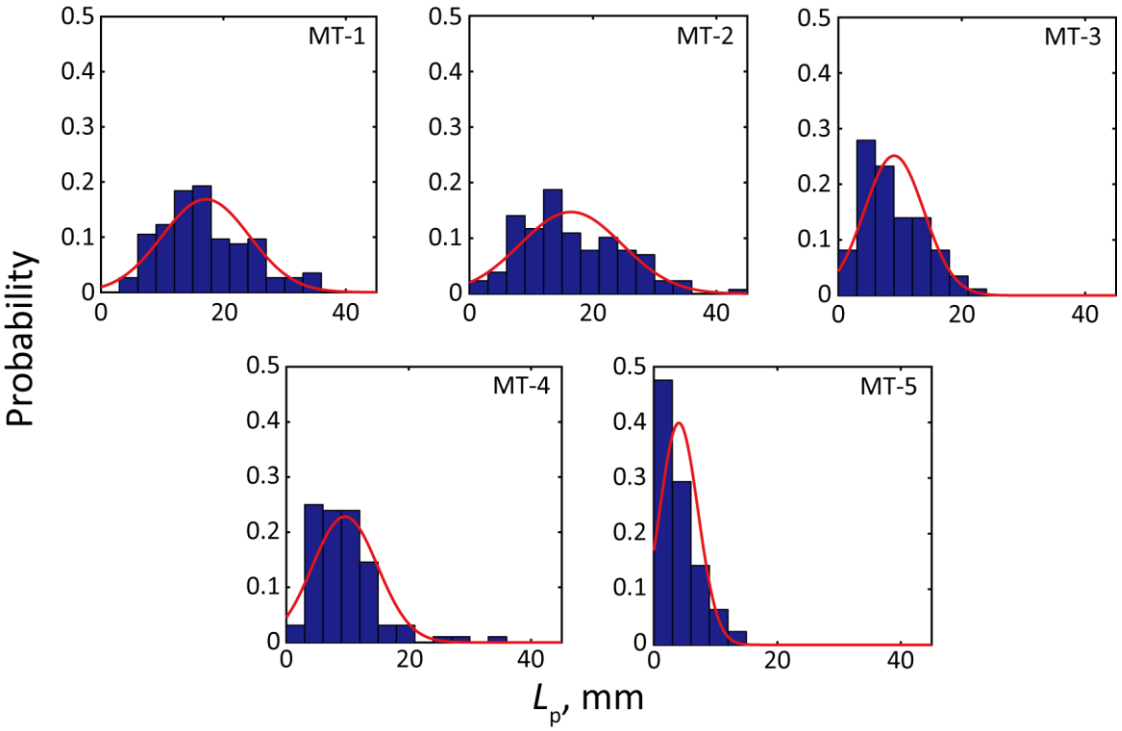

Supplementary Figure 3. | Histograms of L_p for MT-1 to MT-5. Probability distributions are normalized to set the total bin area as one (n = 114 for MT-1, n = 128 for MT-2, n = 86 for MT-3, n = 96 for MT-4, and n = 126 for MT-5). Bin width = 3 mm. Each data set was fit to a Gaussian distribution, $f(L_p)$, as a red line:

$$f(L_p) = \frac{1}{\sigma\sqrt{2\pi}} \exp\left(-\frac{(L_p - \mu)^2}{2\sigma^2}\right) \quad \text{(S13)}$$

to find the mean (μ) and standard deviation (σ) (R^2 = 0.82 for MT-1, R^2 = 0.73 for MT-2, R^2 = 0.79 for MT-3, R^2 = 0.86 for MT-4, and R^2 = 0.80 for MT-5).

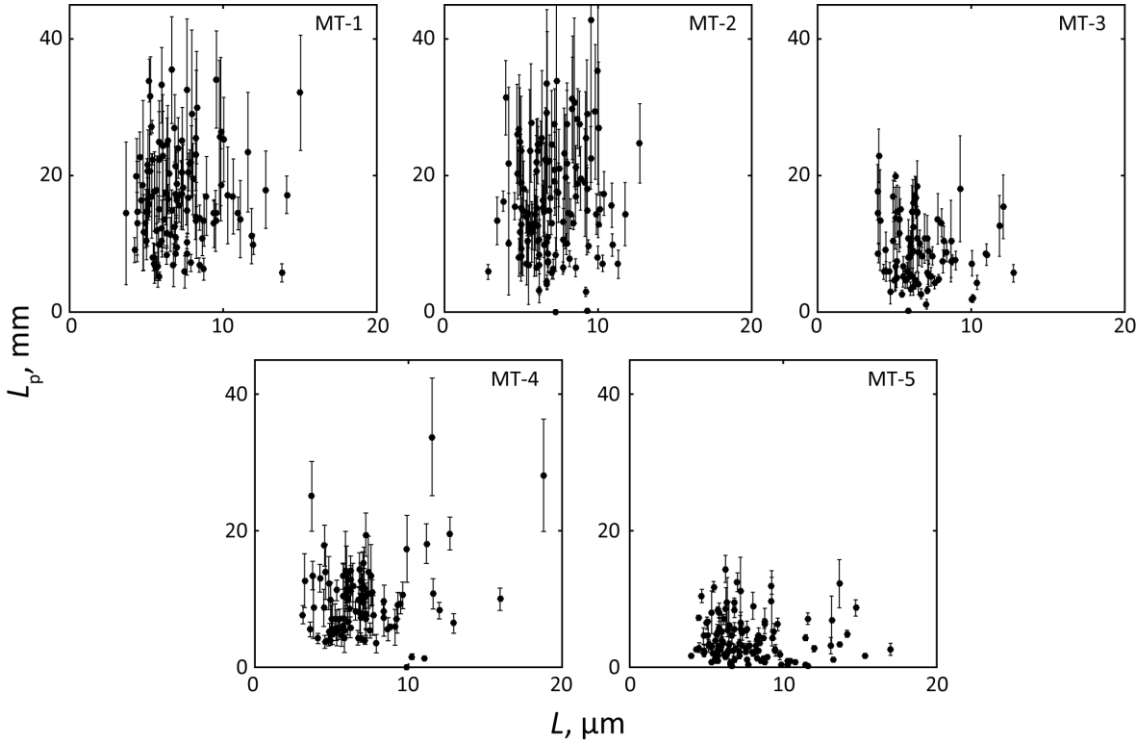

Supplementary Figure 4. | Scatter plots of L_p versus length for MT-1 to MT-5. There was no length dependency of L_p for all MTs by Spearman rank correlation tests at a critical value of $p < 0.05$ (n = 114 for MT-1, n = 128 for MT-2, n = 86 for MT-3, n = 96 for MT-4, and n = 126 for MT-5). Error bars represent the means ± SD.

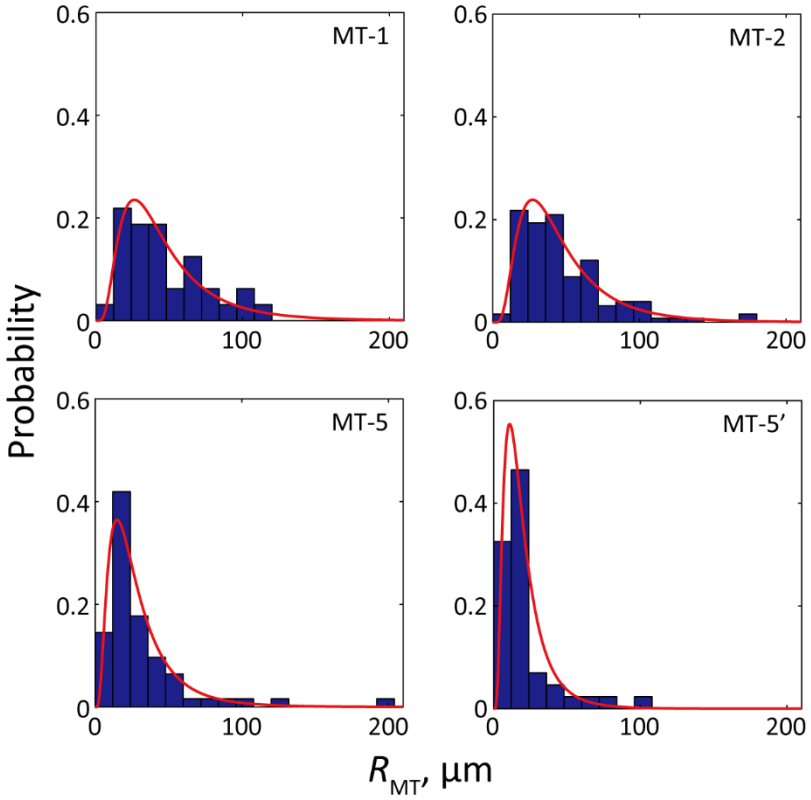

Supplementary Figure 5. | Histograms of R_{MT} for MT-1, MT-2, MT-5, and MT-5′. Probabilities are normalized to set the total bin area as one (n = 32 for MT-1, n = 124 for MT-2, n = 62 for MT-5, and n = 43 for MT-5′). Bin width = 12 μm. Each data set was fit to a log-normal distribution function, $f(R_{MT})$, as a red line:

$$f(R_{MT}) = \frac{1}{\sigma\sqrt{2\pi}} \exp\left(-\frac{(\ln R_{MT} - \mu)^2}{2\sigma^2}\right) \quad \text{(S14)}$$

to find the mean (μ) and the standard deviation (σ) of the natural logarithm of R_{MT} (R^2 = 0.86 for MT-1, R^2 = 0.92 for MT-2, R^2 = 0.96 for MT-5, and R^2 = 0.94 for MT-5′).

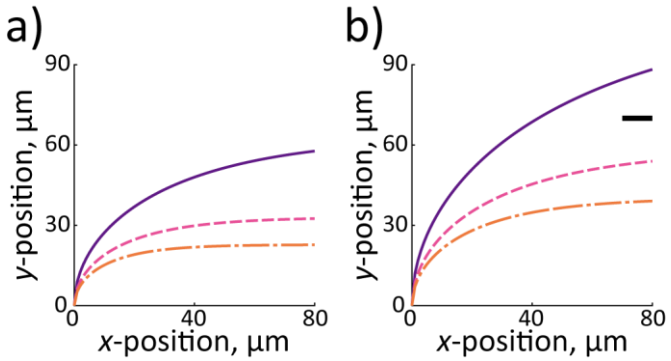

Supplementary Figure 6. | Design of the separation wall. Predicted trajectories of MT-2 (purple, solid lines), MT-5 (pink, broken lines), and MT-5′ (orange, dashed lines) in (**a**) 5.3 kV m^{-1} and (**b**) 3 kV m^{-1}. The black solid line shown in (**b**) represents the determined position of the separation wall.

3. Supplementary Table

Supplementary Table. | Parameter nomenclature.

Variable	Definition	Value	Unit
κ	Flexural rigidity	$1.31–6.88 \times 10^{-23}$	kg m^3 s^{-2}
L_p	Persistence length	3.2–17	mm
L	Microtubule length	-	µm
L_{max}	Upper limit of microtubule length	4.28–6.22	µm
t	Incubation time	0.5–60	min
τ	Time constant for microtubule elongation	1.53–10.8	min
R_{MT}	Trajectory curvature	-	µm
k_B	Boltzmann constant	1.38×10^{-23}	kg m^2 s^{-2} K^{-1}
T	Temperature	300	K
$c_\perp$	Perpendicular Stokes drag coefficient per unit length	1.39×10^{-2}	kg m^{-1} s^{-1}
μ_{el}	Electrophoretic mobility	$2.03/2.09/3.02 \times 10^{-26}$	m^2 V^{-1} s^{-1}
μ_{EOF}	Electroosmotic mobility	1.33×10^{-28}	m^2 V^{-1} s^{-1}
E	Field intensity	$3/5.3 \times 10^3$	V m^{-1}
$<d>$	Average distance between kinesin molecules	1.5–3.0	µm
k_{off}	Detachment rate	-	s^{-1}
y_{max}	Maximum deflection	-	µm
a_n	Mode amplitude	-	$\mu m^{3/2}$
a_n^0	Mode amplitude of initial shape of a microtubule in the absence of thermal energy	-	$\mu m^{3/2}$
r	Correlation coefficient	-	-
τ_n	Correlation time	-	s
γ	Apparent perpendicular drag coefficient	-	s N m^{-2}

4. Supplementary Movies

Supplementary Movie 1. | An example of fluctuating MT-5. The right segment (red) was free to fluctuate under thermal driving. The left segment (light green) was immobilized onto a glass substrate via biotin-streptavidin binding. Images were taken every 400 ms. Playback is 100× real-time (see time stamp). Scale bar = 5 μm.

Supplementary Movie 2. | Sorting of MT-2 and MT-5. Trajectories of MT-2 (yellow) and MT-5 (blue) under an electric field of 3 kV m^{-1}. MT-2 was labelled with rhodamine (red) and MT-5 was labelled with AlexaFluor 488 (green). Images were taken every 3 s. Playback is 200× real-time (see time stamp). Scale bar = 20 μm.

Supplementary Movie 3. | Sorting of MT-2 and MT-5′. Trajectories of MT-2 (yellow) and MT-5′ (blue) under an electric field of 3 kV m^{-1}. MT-2 was labelled with AlexaFluor 488 (green) and MT-5′ was labelled with rhodamine (red). DNA was labelled with AlexaFluor 488 (bright green). Images were taken every 3 s. Playback is 200× real-time (see time stamp). Scale bar = 20 μm.

5. Supplementary References

1. Gittes, F., Mickey, B., Nettleton, J. & Howard, J. Flexural rigidity of microtubules and actin filaments measured from thermal fluctuations in shape. *J. Cell Biol.* **120,** 923-934 (1993).
2. Hawkins, T. *et al.* Perturbations in microtubule mechanics from tubulin preparation. *Cel. Mol. Bioeng.* **5,** 227-238 (2012).
3. Janson, M. E. & Dogterom, M. A bending mode analysis for growing microtubules: evidence for a velocity-dependent rigidity. *Biophys. J.* **87,** 2723-2736 (2004).